

RESEARCH ARTICLE

Standardized Uptake Value in High Uptake Area on Positron Emission Tomography with ^{18}F -FRP170 as a Hypoxic Cell Tracer Correlates with Intratumoral Oxygen Pressure in Glioblastoma

Takaaki Beppu,¹ Kazunori Terasaki,² Toshiaki Sasaki,² Shunrou Fujiwara,¹ Hideki Matsuura,¹ Kuniaki Ogasawara,¹ Koichiro Sera,² Noriyuki Yamada,³ Noriyuki Uesugi,³ Tamotsu Sugai,³ Kohsuke Kudo,⁴ Makoto Sasaki,⁴ Shigeru Ehara,⁵ Ren Iwata,⁶ Yoshihiro Takai⁷

¹Department of Neurosurgery, Iwate Medical University, Uchimaru 19-1, Morioka 020-8505, Japan

²Cyclotron Research Center, Iwate Medical University, Morioka, Japan

³Department of Clinical Pathology, Iwate Medical University, Morioka, Japan

⁴Institute for Biomedical Sciences, Iwate Medical University, Morioka, Japan

⁵Department of Radiology, Iwate Medical University, Morioka, Japan

⁶Cyclotron and Radioisotope Center (CYRIC), Tohoku University, Sendai, Japan

⁷Department of Radiology and Radiation Oncology, Hirosaki University Graduate School of Medicine, Hirosaki, Japan

Abstract

Purpose: The aim of this study was to clarify the reliability of positron emission tomography (PET) using a new hypoxic cell tracer, 1-(2-[^{18}F]fluoro-1-[hydroxymethyl]ethoxy)methyl-2-nitroimidazole (^{18}F -FRP170).

Procedures: Twelve patients with glioblastoma underwent ^{18}F -FRP170 PET before tumor resection. Mean standardized uptake value (SUV) and normalized SUV were calculated at regions within a tumor showing high (high-uptake area) and relatively low (low-uptake area) accumulations of ^{18}F -FRP170. In these areas, intratumoral oxygen pressure (tpO₂) was measured using microelectrodes during tumor resection.

Results: Mean tpO₂ was significantly lower in the high-uptake area than in the low-uptake area. A significant negative correlation was evident between normalized SUV and tpO₂ in the high-uptake area.

Conclusion: The present findings suggest that high accumulation on ^{18}F -FRP170 PET represents viable hypoxic tissues in glioblastoma.

Key words: F-FRP170, PET, Hypoxia, Glioblastoma, Oxygen pressure, HIF1- α

Abbreviation: Cu-ATSM, ⁶⁴Cu-diacetyl-bis(N4-methylthiosemicarbazone); ^{18}F -FRP170, 1-(2-[^{18}F]fluoro-1-[hydroxymethyl]ethoxy)methyl-2-nitroimidazole; ^{18}F -FAZA, 1- α -D-(5-deoxy-5-5-[^{18}F]-fluoroarabinofuranosyl)-2-nitroimidazole; ^{18}F -FMISO, [^{18}F]fluoromisonidazole; Gd-T1WI, Gadolinium-enhanced T1-weighted imaging; HIF, Hypoxic-inducible factor; MRI, Magnetic resonance imaging; ROI, Region of interest; T2WI, T2-weighted imaging; PET, Positron emission tomography; VEGF, Vascular endothelial growth factor

Introduction

Almost all malignant solid tumors include hypoxic cells due to both excessive consumption and insufficient supply of oxygen within the tumor. Intratumoral hypoxia induces various biological characteristics in tumors. For instance, hypoxia in tumor activates the hypoxia-responsive elements such as hypoxia-inducible factors (HIFs), leading to transcription of target genes including vascular endothelial growth factor (VEGF). VEGF induces angiogenesis, and is also closely related to the proliferation and invasion of tumor. Gene instability caused by hypoxia must affect the differentiation of tumor cells. Intratumoral hypoxic conditions are disadvantageous in term of the production of peroxide radicals, which induces DNA damage under irradiation. Cancer stem cells existing within hypoxic tumor tissue have also been considered to represent a likely cause of radioresistance [1–3]. In glioblastoma, hypoxic conditions play a key role in the development of tumor characteristics. Neuroimaging enabling minimally invasive, objective, and quantitative evaluation of hypoxic conditions in glioblastoma would offer many clinical benefits in terms of diagnosis, selection of treatment, and prediction of prognosis.

Positron emission tomography (PET) using hypoxic cell tracers offers an attractive method for detecting hypoxic cells because it is simple, low-invasive, repeatable, and not limited in applicability to superficial tumors [4]. So far, hypoxic cells in brain tumors have been detected using PET with hypoxic cell tracers such as [^{18}F]fluoromisonidazole (^{18}F -FMISO) [5–7], 1- α -D-(5-deoxy-5-5-[^{18}F]-fluoroarabino-furanosyl)-2-nitroimidazole (^{18}F -FAZA) [8], and ^{64}Cu -diacetyl-bis(N4-methylthiosemicarbazone) (Cu-ATSM) [9, 10]. A new hypoxic cell tracer, 1-(2-[^{18}F]fluoro-1-[hydroxymethyl]ethoxy)methyl-2-nitroimidazole (^{18}F -FRP170), has recently been identified [11, 12]. PET using ^{18}F -FRP170 (^{18}F -FRP170 PET) has already been performed for detecting hypoxic cells in malignant brain tumors, and the potential of this new tracer has been documented [13]. Several studies assessing intratumoral oxygen condition using electrodes or other methods have confirmed reliability of PET with various hypoxic cell tracers other than ^{18}F -FRP170 [14–17]. However, whether areas of high accumulation on ^{18}F -FRP170 PET really represent tissues including hypoxic cells, and to what degree areas of high accumulation represent regions under hypoxic conditions have remained unclear. The aim of this study was to confirm the reliability of ^{18}F -FRP170 PET for detecting hypoxic cells. We therefore compared standardized uptake value (SUV) measured on ^{18}F -FRP170 PET with intratumoral oxygen pressure (tpO₂) within glioblastoma measured using oxygen microelectrodes during tumor resection. Furthermore, we performed immunohistochemical detection HIF-1, a heterodimeric nuclear transcription factor playing a critical role in cellular response to low oxygen pressure [18], in tissues corresponding to the regions of interest (ROIs) on ^{18}F -FRP170 PET images.

Materials and Methods

Patients

All study protocols were approved by the Ethics Committee of Iwate Medical University, Morioka, Japan (No. H22-70). Patients recruited to this study were admitted to Iwate Medical University Hospital between April 2008 and December 2012. Entry criteria for the study were: patients ≥ 20 years old with non-treated glioblastoma localized in cerebral white matter other than the brain stem or cerebellum, performance of ^{18}F -FRP170 PET and measurement of absolute oxygen pressure within the tumor according to the study protocol, and voluntary provision of written informed consent to participate. Preoperative diagnosis was based on present history and findings from conventional magnetic resonance imaging (MRI) on admission, and final diagnosis of glioblastoma was made based on histological features after surgery. Twelve patients (ten men, two women, mean age, 63 ± 13.7 years) were enrolled after excluding patients who did not meet the entry criteria (Table 1).

^{18}F -FRP170 PET

Within 7 days (mean, 4.3 ± 2.4 days) before surgery for tumor resection, both conventional MRI including gadolinium-enhanced T1-weighted imaging (Gd-T1WI) and ^{18}F -FRP170 PET were performed. The ^{18}F -FRP170 was synthesized using on-column alkaline hydrolysis according to the methods described by Ishikawa et al. [12]. The final formulation for injection was formed in normal saline containing 2.5 %v/v ethanol using solid-phase extraction techniques. At 60 min after intravenous injection of approximately 370 MBq (mean, 5.9 ± 1.8 MBq/kg) of ^{18}F -FRP170, PET was performed using a PET/computed tomography (CT) system (SET3000 GCT/M; Shimazu, Japan). On ^{18}F -FRP170 PET, ROIs of 10 mm in diameter were placed at areas of high accumulation (high-uptake area) and relatively low accumulation (low-uptake area) within the tumor bulk (Fig. 1a, b). These ROIs were placed at regions as close to the brain surface as possible to allow easy and safe insertion of microelectrodes for measuring oxygen pressure during surgery. A ROI was also placed in apparent normal cerebral white matter of the contralateral side. SUV for each ROI was automatically determined. Although both mean and maximal values of SUV in ROI were measured, we defined the mean value of SUV as “SUV” in this study. The normalized SUV, defined as SUV for each high- or low-uptake area divided by SUV for the apparent normal cerebral white matter of the contralateral hemisphere, was also calculated.

Immediately before surgery for each patient, we created a fusion image that combined a three-dimensional ^{18}F -FRP170 PET image with Gd-T1WI using a surgical navigation system (Stealth Station TRIA plus; Medtronic, Minneapolis, MN) in the operation room. On the fusion image, both high- and low-uptake areas were identified stereotactically for each patient (Fig. 2a–d).

Measurement of Intratumoral Oxygen Pressure During Surgery

Measurement of tpO₂ was performed during surgery for aggressive tumor resection. The tpO₂ level was measured using disposable

Table 1. Patient characteristics and measurement data

No.	Sex	Age (year)	Location	SUV			Normalized SUV		tpO ₂ (mmHg)		PaO ₂ (mmHg)	HIF-1α staining
				High uptake	Low uptake	ANWM	High uptake	Low uptake	High uptake	Low uptake		
1	M	76	Parietal lobe	0.99	0.54	0.54	1.83	1.00	23	44	157	–
2	M	81	Parietal lobe	2.22	1.39	1.04	2.13	1.34	16	45	128	–
3	M	59	Frontal lobe	1.46	1.16	0.87	1.69	1.33	28	56	176	–
4	F	61	Frontal lobe	1.10	0.87	0.74	1.49	1.18	32	54	145	–
5	M	75	Parietal lobe	1.83	1.11	0.83	2.20	1.34	16	33	143	–
6	F	54	Parietal lobe	1.43	0.82	0.62	2.31	1.32	30	54	134	–
7	M	64	Temporal lobe	1.62	1.00	0.72	2.25	1.39	15	27	158	+
8	M	54	Occipital lobe	1.50	1.01	0.76	1.97	1.33	17	35	120	+
9	M	67	Frontal lobe	1.84	1.46	1.13	1.63	1.29	25	36	132	+
10	M	76	Temporal lobe	1.90	0.92	0.77	2.47	1.19	15	26	124	+
11	M	58	Frontal lobe	1.37	1.25	0.90	1.52	1.39	24	34	137	+
12	M	31	Frontal lobe	1.66	1.11	0.87	1.91	1.28	20	37	148	+

ANWM apparent normal white matter, tpO₂ intratumoral oxygen pressure

Clark-type electrodes (UOE-04TS; Unique Medical, Tokyo, Japan) at the tip of a sensor (Teflon-coated tube; diameter, 0.4 mm; length, 10 mm). Immediately before surgery, electrodes were sterilized by immersion in a solution of 2.25 w/v% glutaraldehyde and buffer for 2 h, then washed with sterilized physiological saline solution. The electrode was then connected to a digital oxygen pressure monitor (POG-203; Unique Medical) to calibrate the value of oxygen pressure to 150 mmHg in a sterilized physiological saline solution prior to insertion into the tumor. After craniotomy, we stereotactically inserted a needle-shaped navigating marker of 2 mm in diameter into the center region of the high-uptake area where the ROI had been placed before surgery through the dura mater, while we observed the localization of the tip of the marker in the tumor on the monitor of the surgical navigation system (Fig. 2c, d). After removal of the navigation marker, we immediately inserted the electrode along the same trajectory through the dura mater, with the tip of the electrode placed within tumor tissue of the high-uptake area. A digital monitor was then used to measure tpO₂. We observed tpO₂ value gradually declined from 150 mmHg while rising and falling on the digital monitor, and defined the minimum value as the absolute tpO₂ value at the high-uptake area for each patient. After completely washing and calibrating the value of oxygen pressure to 150 mmHg in a sterilized physiological saline solution, the same procedure described above was performed to measure tpO₂ in the low-uptake area. During measurements of tpO₂, arterial oxygen pressure (PaO₂) was measured using arterial blood obtained from the radial artery. After measuring tpO₂ and removing the electrode, we inserted a needle for biopsy along a trajectory to obtain tumor tissues from the high- and low-uptake areas in six patients. In all cases, the tumor was successfully removed after completing the procedures described above.

HIF-1α Immunohistochemistry

Immunohistochemical staining of HIF-1α was performed on specimens obtained from tumor resection for six patients. From all specimens in both high- and low-uptake areas, paraffin-embedded tissue sections of 3-μm-thickness were collected onto 3-aminopropyltriethoxysilane-coated glass slides. The dewaxed preparations were given microwave pretreatment for 30 min in sodium citrate. The preparations were incubated for 60 min using

rabbit anti-HIF-1α monoclonal antibody (clone, H1α67; Novus Biologicals, Littleton, CO) at 1:200 dilution. Preparations were incubated using peroxidase-based EnVision kits (Dako Japan, Tokyo, Japan) as the secondary antibody, then immersed in diaminobenzidine/H₂O₂ solution for colored visualization. Finally, preparations were counterstained with hematoxylin.

We observed the staining attitude of HIF-1α in tumor cells for all patients. We also evaluated the HIF-1α staining indices for each high- or low-uptake area for each patient, defined as the percentage of cells showing nuclear staining as determined by counting approximately 1,000 cells under light microscopy (×400 magnification).

Statistical Analyses

In all patients, differences in SUV, normalized SUV, and HIF-1α staining index were compared between high- and low-uptake areas using the Mann–Whitney *U* test. Differences in intratumoral pO₂ between high- and low-uptake areas were also compared in all patients using the Mann–Whitney *U* test. Correlations between PaO₂ and tpO₂ and between normalized SUV and tpO₂ for all patients were analyzed in each high- and low-uptake area using Pearson's correlation coefficient test.

Results

Scanning at 60 min after intravenous injection of tracer provided fine contrast images that enabled visual differentiation between high- and low-uptake areas in all patients. In eight patients with glioblastoma presenting a central necrotic region, ¹⁸F-FRP170 was partially accumulated in the intermediate layer between the deep layer surrounding the central necrotic region and the outer layer within the peripheral region of tumor involved in lesion enhancement on Gd-T1WI (Fig. 1a, b). Fusion images combining Gd-T1WI and ¹⁸F-FRP170 PET provided precise locations of both high- and low-uptake regions during surgery, and allowed us to successfully insert electrodes and obtain the

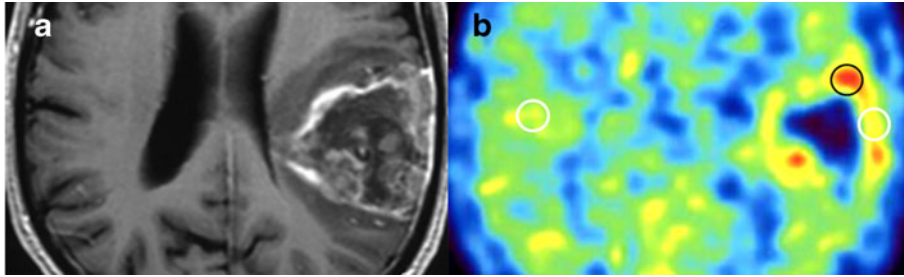


Fig. 1. Typical findings of ^{18}F -FRP170 PET in glioblastoma with a large area of central necrosis in Case 1. High-uptake areas are seen partially in the area between the outer peripheral region showing enhancement on Gd-T1WI and a deeper region adjacent to the central necrotic region. ROIs were placed on a high-uptake area (*black circle*) and a relatively low-uptake area (*white circle*) within the tumor bulk showing enhancement on Gd-T1W, and also on apparent normal white matter of the contralateral hemisphere (*white circle*). **a** Gd-T1WI, **b** ^{18}F -FRP170 PET.

sampling tissues (Fig. 2a–d). No patient presented with any complications due to ^{18}F -FRP170 PET.

Mean SUV for high-uptake areas, low-uptake areas, and contralateral normal white matter regions were 1.58 ± 0.35 , 1.05 ± 0.25 , and 0.82 ± 0.16 , respectively. Significant differences in mean SUV were found between high- and low-uptake areas ($p=0.001$), between high-uptake areas and normal white matter ($p<0.001$), and between low-uptake

areas and normal white matter ($p=0.01$), although SUV values in the three groups overlapped (Fig. 3a). Mean normalized SUV for the high- and low-uptake areas were calculated as 1.95 ± 0.33 and 1.28 ± 0.11 , respectively. Mean normalized SUV for the high-uptake area differed significantly ($p<0.001$) and clearly from that of the low-uptake area, with a cut-off level of around 1.4 (Fig. 3b). Mean tpO_2 was significantly lower in high-uptake areas ($21.7 \pm$

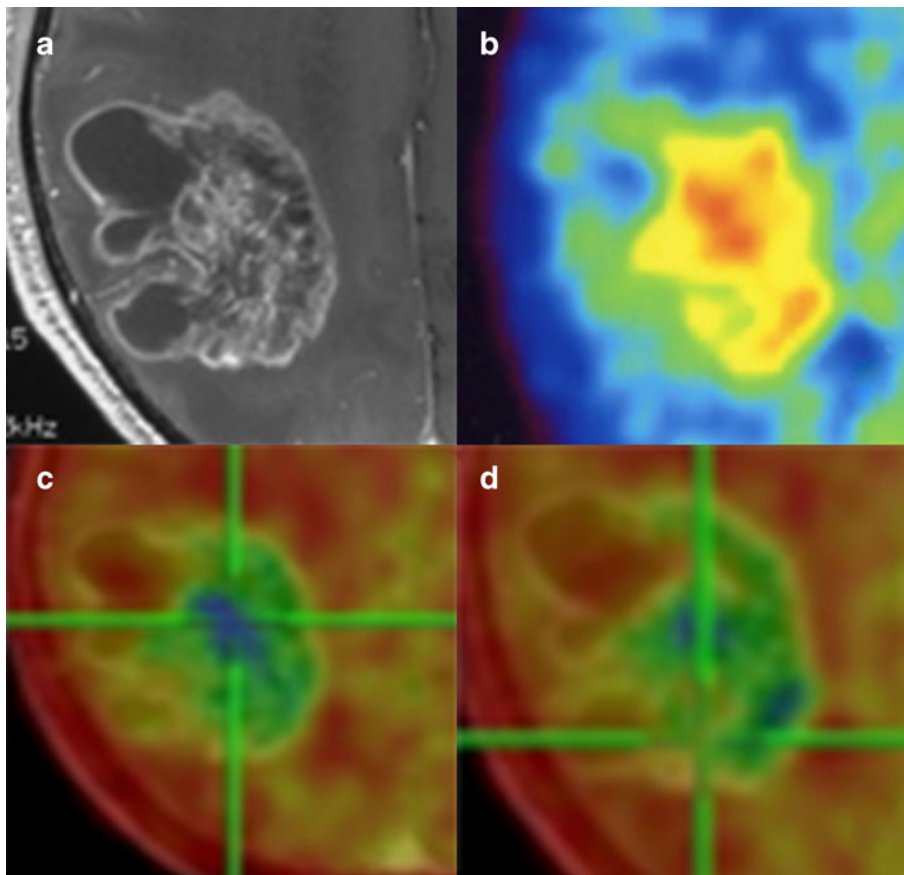


Fig. 2. High- and low-uptake areas were stereotactically localized on fusion images combining Gd-T1WI (**a**) and ^{18}F -FRP170 PET (**b**) for Case 5, to identify tumor tissues corresponding to ROIs. On fusion images, high- and low-uptake areas were depicted as bluish regions (**c**) and greenish regions (**d**), respectively.

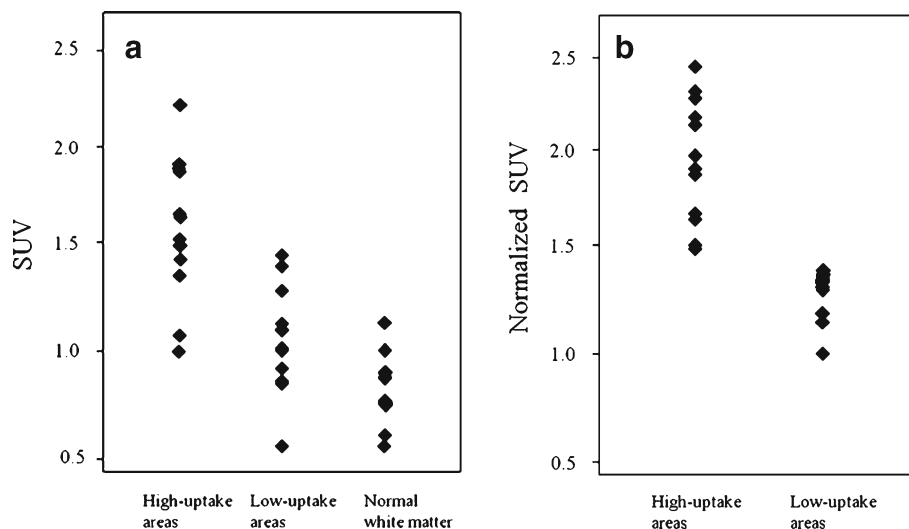


Fig. 3. **a** Differences in SUV among the high-uptake area, low-uptake area, and apparent normal white matter. **b** Difference in normalized SUV between high- and low-uptake areas.

6.2 mmHg) than in low-uptake areas (40.1 ± 10.4 mmHg; $p < 0.001$, Fig. 4). In terms of the relationship between normalized SUV and tpO_2 in all patients, a significant negative correlation was found in high-uptake areas ($r = -0.64$, $p = 0.03$), whereas no significant correlation was identified in low-uptake

areas (Fig. 5a, b). No significant correlations between PaO_2 and tpO_2 were found in either high- or low-uptake areas (not shown).

On specimens obtained from high-uptake areas, HIF-1 α was clearly detectable in nuclei in all six patients, with three patients also showing HIF-1 α staining in cytoplasm. On the other hand,

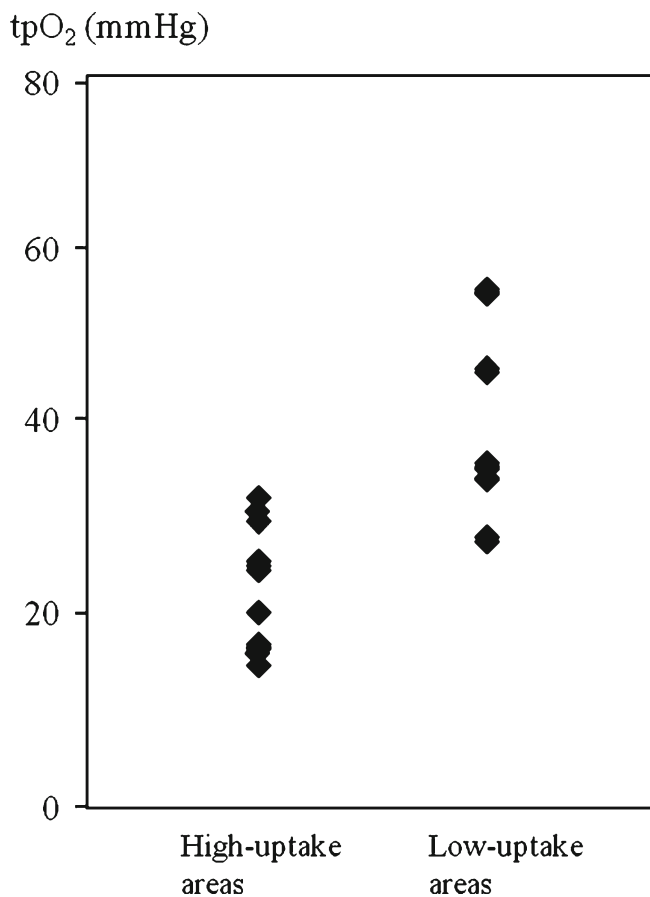


Fig. 4. Difference in tpO_2 between high- and low-uptake areas.

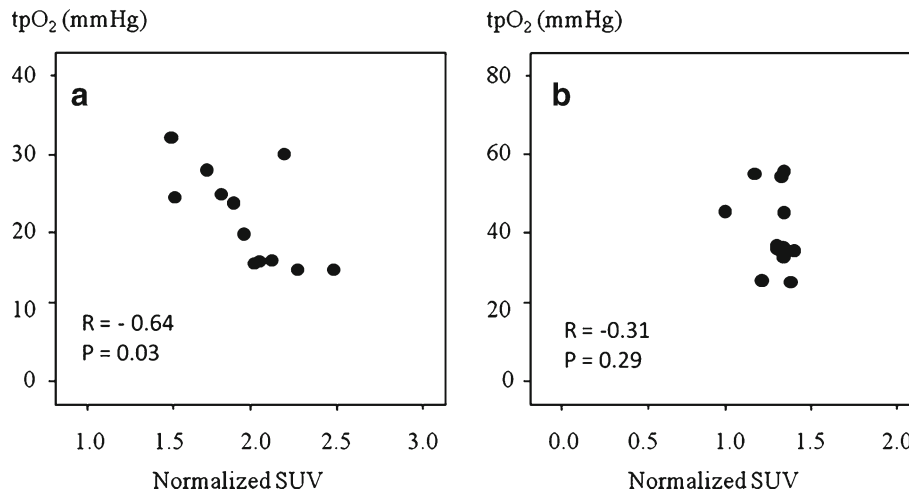


Fig. 5. Correlations between normalized SUV and tpO₂ in high-uptake areas (a) and low-uptake areas (b).

specimens from low-uptake areas showed three different patterns, with HIF-1 α staining only cytoplasm in three patients, and both nuclei and cytoplasm in two patients. In the remaining patient, few barely surviving cells with HIF-1 α staining were seen within a wide area of necrotic tissue (Fig. 6a–d). HIF-1 α staining indices ranged from 35.2 to 63.5 % in high-uptake

areas, and from 8.9 to 35.9 % in low-uptake areas. Mean HIF-1 α staining index was significantly higher in high-uptake areas (mean, 53.0 ± 10.2 %) than in low-uptake areas (mean, 18.9 ± 9.5 %). Notably, HIF-1 α staining index was markedly low (8.9 %) in necrotic tissue obtained from a low-uptake area in one patient.

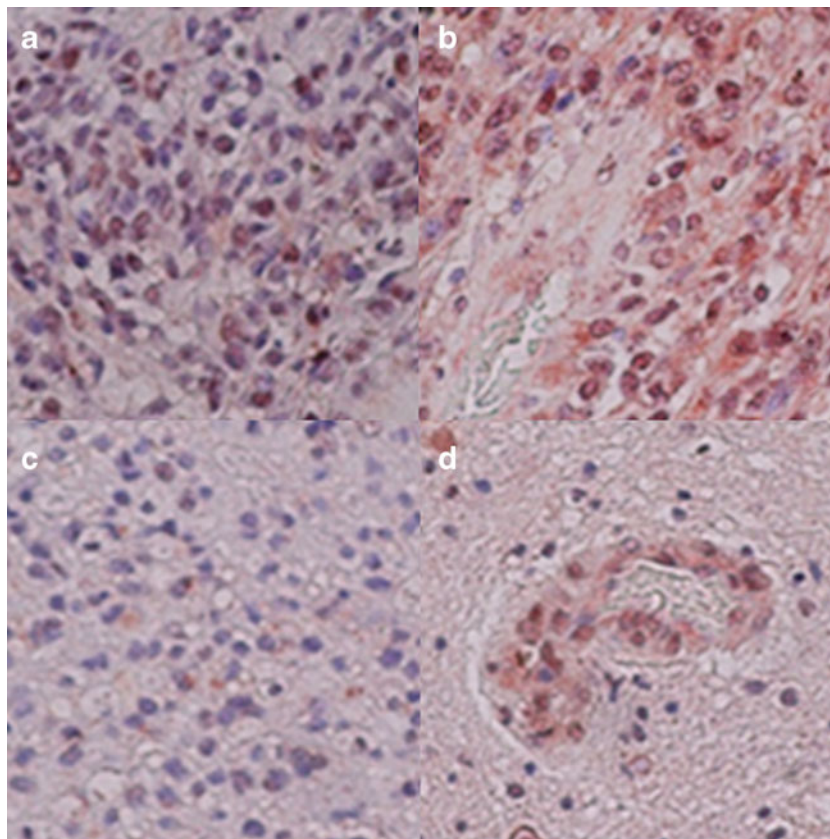


Fig. 6. Findings for HIF-1 α immunostaining of tissues from high-uptake areas (a, b) and low-uptake areas (c, d). a HIF-1 α was strongly detected in nuclei in all patients. b HIF-1 α was stained in both cytoplasm and nuclei in three patients. c HIF-1 α was stained only in cytoplasm in three patients. d A few HIF-1 α -stained cells were seen within a wide necrotic tissue in one patient.

Discussion

The present study showed that mean values of both SUV and normalized SUV were significantly higher in high-uptake areas than in low-uptake areas. In particular, normalized SUV values in high-uptake areas were absolutely higher than those in low-uptake areas. In this study, approximately 370 MBq of ¹⁸F-FRP170 was administered intravenously for all patients, according to a report by Shibahara et al. [13]. Absolute SUV might thus have been subtly influenced by the delivered volume of tracer into the tumor as determined by individual parameters, such as body size, cardiac output volume, and blood pressure. As normalization of absolute SUV can eliminate differences in these factors, we emphasize the importance of estimation using normalized SUV. In the present study, tpO₂ did not correlate with PaO₂ at all. Two previous reports examining both tpO₂ in brain tumors and PaO₂ could not find any relationship between these measured values, although correlations were not estimated statistically [19, 20]. Our results support those previous reports and indicate that tpO₂ was not influenced by PaO₂ during surgery. Values of tpO₂ were significantly lower in high-uptake areas (21.7 ± 6.2 mmHg) than in low-uptake areas (40.1 ± 10.4 mmHg). Furthermore, a significant correlation was found between normalized SUV and tpO₂ in high-uptake areas. These results indicate that high-uptake areas where ¹⁸F-FRP170 accumulates show relatively more hypoxic conditions than low-uptake areas, suggesting the reliability of findings from ¹⁸F-FRP170 PET.

Selective accumulation of ¹⁸F-FRP170 in hypoxic cells has been considered to proceed as follows. First, the nitroimidazole moiety in ¹⁸F-FRP170 is responsible for the initial accumulation in hypoxic cells. After passive diffusion inside the cells, enzymatic nitroreduction by nitroreductase results in nitroimidazole changing to radical anions. Under normoxic conditions, these radical anions are reoxidized and diffuse out of the cells, whereas products comprising radical anions covalently bound to intracellular macromolecules are trapped within cells under hypoxic conditions [13, 21–23]. As a result, ¹⁸F-FRP170 can accumulate only within viable and active hypoxic cells, but cannot accumulate within normoxic cells or even hypoxic cells with low metabolism such as apoptotic or necrotic cells. A previous report assessing accumulation of ¹⁸F-FRP170 in a rat model of ischemic myocardium using autoradiography documented that ¹⁸F-FRP170 was observed only within viable hypoxic myocardial cells [11]. As absolute SUV must correlate with the concentration of PET tracer within the tissue, SUV on ¹⁸F-FRP170 PET should increase with a higher density of viable hypoxic cells within the tissues of the ROI. We think that such high-uptake areas represent glioblastoma tissue comprising a high density of viable hypoxic cells. In contrast, tissues of low-uptake areas might represent low densities of viable hypoxic cells. In other words, a majority of cells in low-uptake areas could not accumulate ¹⁸F-

FRP170 because of the presence of either viable cells containing relatively higher tpO₂ than high-uptake area or low metabolic-hypoxic cells degenerating in apoptosis or necrosis. The oxygen environment may thus differ substantially among different regions in low-uptake areas, despite the similar content of viable hypoxic cells. Indeed, tpO₂ levels showed a wide range in low-uptake areas, with a large standard deviation (Fig. 4). This might be one reason for the lack of significant correlation between tpO₂ levels and normalized SUV in low-uptake areas. As intratumoral hypoxia is generally considered to result from insufficient oxygen supply paralleling the distance from normal vessels surrounding the tumor, intratumoral oxygen pressure should be higher in more peripheral regions of glioblastoma that are also supplied with blood from normal vessels surrounding the tumor bulk [24, 25]. On PET in the present study, interestingly, high-uptake areas were observed partially within the intermediate layer of enhancing lesions on Gd-T1WI, and low-uptake areas were seen not only in the peripheral layer external to the intermediate layer containing high-uptake areas but also in the inner core layer adjacent to the central necrosis deep to the intermediate layer (Fig. 1b). We assumed that low-uptake areas in both peripheral and inner core layers might contain little ¹⁸F-FRP170-accumulating hypoxic cells, but the peripheral layers included many viable cells at relatively high oxygen pressure, while the inner core comprises low metabolic-hypoxic cells undergoing degenerative apoptosis or necrosis. Remaining low-uptake areas in the intermediate layer probably represent mixture of the two histological types described above. Pistollato et al. [26] evaluated biological characteristics in tissues isolated from three concentric layers (core, intermediate, and peripheral layers) in glioblastoma. The core and intermediate layers showed expression of HIF-1α as a hypoxic cell marker, whereas the peripheral layer did not express HIF-1α, but showed expressions of glial fibrillary acidic protein and β-III-tubulin as mature neural cell markers. In addition, core and intermediate layers contained more glioblastoma stem cells, which are well known to be frequently seen in hypoxic niches. These results suggest that inner core and peripheral layers depicted as low-uptake areas on ¹⁸F-FRP170 PET in the present study are likely to exhibit hypoxic and relatively normoxic conditions, respectively.

Hypoxic condition rapidly induces overexpression of HIF-1α for transcribing target genes such as vascular endothelial growth factor to induce angiogenesis, as countermeasures against hypoxic conditions. Under normoxic conditions, prolyl hydroxylation is induced in HIF-1α, allowing binding to the von-Hippel-Lindau protein, which mediates ubiquitination of HIF-1α and subsequent proteasomal degeneration in the cytoplasm. However, under hypoxic conditions, the oxygen requiring prolyl hydroxylase remains inactive, resulting in accumulation of the constitutively expressed HIF-1α protein in cytoplasm. This subunit is phosphorylated and translocated to the nucleus, where it dimerizes with the HIF-1β subunit, binding to the hypoxia-

response elements upstream of HIF-1-regulated target genes [27]. Therefore, increasingly activated-HIF-1 α induced by hypoxia accumulates in the nucleus. In this study, all specimens obtained from high-uptake areas clearly showed nuclear staining for HIF-1 α , whereas this finding was seen in low-uptake areas in only two patients. Furthermore, mean HIF-1 α staining index determined by the percentage of cells showing nuclear staining was significantly higher in high-uptake areas than in low-uptake areas. Necrotic tissue obtained from a low-uptake area of one patient showed an extremely low HIF-1 α staining index. These findings might support the concept that high-uptake areas represent more hypoxic regions with a high density of viable and active hypoxic cells. Tissues of low-uptake areas were not obtained from deeper than high-uptake areas but rather from the same depth or more externally during surgery in all six patients. As a result, HIF-1 α was also detected in the low-uptake areas of all patients, but showed a greater variety of features than high-uptake areas. These findings support the possibility that low-uptake areas comprised either numerous viable cells under conditions of relatively higher oxygen pressure or low metabolic hypoxic cells under degenerative apoptosis or necrosis.

In the present study, PET at 60 min after intravenous injection of ^{18}F -FRP170 could provide visually fine-contrast PET images. Shidehara et al. [13] reported fine-contrast color images provided by imaging at 120 min after injection of ^{18}F -FRP170 in patients with malignant brain tumor. Kaneta et al. [21] reported that imaging results at 120 min after injection of ^{18}F -FRP170 for patients with lung cancer contributed only a slightly higher tumor/blood ratio when compared with that at 60 min, and concluded that imaging at 60 min after administration was clinically sufficient for assessing hypoxic cells in tumors. The present study supported these recommendations by Kaneta et al. In an experimental study using mice bearing cultured cancer cells, ^{18}F -FAZA displayed significant higher tumor-to-background ratios compared with ^{18}F -FMISO and another azomycin-based nucleoside, iodoazomycin arabinoside, labeled with ^{124}I (^{124}I -IAZA), when scanning for all tracer was fixed in 3 h post-injection [28]. Clinically, PET imaging with ^{18}F -FMISO and ^{18}F -FAZA has usually been scanned at 120–140 [5–7] and 120–210 min [8] after administration, respectively. Although no previous reports have directly compared ^{18}F -FRP170 PET and ^{18}F -FMISO PET images, ^{18}F -FRP170 PET has been considered superior in terms of fine contrast and rapid clearance from blood [21]. The short duration for imaging could represent an additional advantage to ^{18}F -FRP170 PET.

Some limitations regarding the interpretation of study results must be considered for this study. First, the sample size in this study was small. Additional studies of a larger number of patients with glioblastoma are needed. Second, use of smaller ROIs might provide more rigorous results in comparisons among SUV, tpO_2 , and histological features. However, in this study, we placed relatively huge ROIs of

10 mm in diameter to avoid misplacement of microelectrodes within the ROI and sampling error of tumor tissues corresponding to the ROI. These issues could represent factors contributing to make maximum SUV within the ROI unsuitable for use in this study. In short, errors involving differences between pinpoint regions for insertion of electrode and maximum SUV could easily be anticipated. Third, direct tpO_2 measurements using microelectrodes available differ in sensitivity, accuracy, ability to measure oxygen availability among types of probe used, and impossibility in differentiation between hypoxic and necrotic tissues, although this technique is commonly considered a gold standard [4]. Other techniques indirectly measuring oxygen through reduced drug levels, hemoglobin saturation, or perfusion have been proposed. However, indirect measurements, although valuable, require a set of assumptions to relate the measurement to tpO_2 or oxygen concentration [4]. Fourth, measurement of tpO_2 using electrodes in this study did not strictly represent intracellular oxygen pressure, but rather the oxygen pressure of tissue containing hypoxic cells. However, tpO_2 as measured in this study would correlate with intracellular oxygen pressure, as intracellular oxygen pressure is regulated by extracellular conditions. Fifth, measured tpO_2 values in this study were relatively higher (21.7 ± 6.2 mmHg in high-uptake areas and 40.1 ± 10.4 mmHg in low-uptake areas) than in previous reports of direct measurement using Eppendorf oxygen electrodes in malignant brain tumors, where mean tpO_2 has been reported as approximately ≤ 20 mmHg [20, 24, 29]. In particular, mean value in low-uptake areas was significantly higher. However, mean tpO_2 in low-uptake areas was lower than that of brain tissue around the tumor (59.8 ± 6.5 mmHg) in a previous report [20]. In previous reports regarding oxygen pressure at high-uptake areas on ^{18}F -FMISO PET in animal tumor models, measurements using Eppendorf electrodes showed a high frequency of $\text{tpO}_2 \leq 10$ mmHg [15, 30, 31]. Although the reasons for this contradiction are not entirely clear, we consider these results may have arisen from differences in the electrodes used, or from the inflow of a small amount of air into the trajectory when electrodes were inserted immediately after removal of the navigation marker with a larger diameter than the electrode. However, as this issue applied to measurements of tpO_2 for all patients in this study, the findings of higher tpO_2 in high-uptake areas compared to low-uptake areas appear valid.

Conclusions

Findings of a significant correlation between normalized SUV and tpO_2 , and strong nuclear immunostaining for HIF-1 α in areas of high ^{18}F -FRP170 accumulation, suggest that high-uptake areas on ^{18}F -FRP170 PET represent high densities of viable hypoxic cells, at least in glioblastoma. However, interpretation of low-uptake areas is more complicated, given the likelihood that these lesions comprise

various oxygen environments containing low densities of viable hypoxic cells.

Acknowledgments. This study was supported in part by Grant-in-Aid for Strategic Medical Science Research Center for Advanced Medical Science Research from the Ministry of Science, Education, Sports and Culture, Japan.

Conflict of Interest. The authors declare that they have no conflicts of interest.

References

- Jensen RL (2009) Brain tumor hypoxia: tumorigenesis, angiogenesis, imaging, pseudoprogression, and as a therapeutic target. *J Neurooncol* 92:317–335
- Jensen RL (2006) Hypoxia in the tumorigenesis of gliomas and as a potential target for therapeutic measures. *Neurosurg Focus* 20:E24
- Rich JN (2007) Cancer stem cells in radiation resistance. *Cancer Res* 67:8980–8984
- Mendichovszky I, Jackson A (2011) Imaging hypoxia in gliomas. *Br J Radiol* 84(2):S145–S158
- Eschmann SM, Paulsen F, Reimold M et al (2005) Prognostic impact of hypoxia imaging with 18F-misonidazole PET in non-small cell lung cancer and head and neck cancer before radiotherapy. *J Nucl Med* 46:253–260
- Kawai N, Maeda Y, Kudomi N et al (2011) Correlation of biological aggressiveness assessed by 11C-methionine PET and hypoxic burden assessed by 18F-fluoromisonidazole PET in newly diagnosed glioblastoma. *Eur J Nucl Med Mol Imaging* 38:441–450
- Swanson KR, Chakraborty G, Wang CH et al (2009) Complementary but distinct roles for MRI and 18F-fluoromisonidazole PET in the assessment of human glioblastomas. *J Nucl Med* 50:36–44
- Postema EJ, McEwan AJ, Riauka TA et al (2009) Initial results of hypoxia imaging using 1- α -D:-(5-deoxy-5-[¹⁸F]-fluoroarabinofuranosyl)-2-nitroimidazole (¹⁸F-FAZA). *Eur J Nucl Med Mol Imaging* 36:1565–1573
- Sheehan JP, Popp B, Monteith S et al (2011) Trans sodium crocetin: functional neuroimaging studies in a hypoxic brain tumor. *J Neurosurg* 115:749–753
- Tateishi K, Tateishi U, Sato M et al (2013) Application of ⁶²Cu-diacetyl-bis (N4-methylthiosemicarbazone) PET imaging to predict highly malignant tumor grades and hypoxia-inducible factor-1 α expression in patients with glioma. *AJNR Am J Neuroradiol* 34:92–99
- Kaneta T, Takai Y, Kagaya Y et al (2002) Imaging of ischemic but viable myocardium using a new 18F-labeled 2-nitroimidazole analog, 18F-FRP170. *J Nucl Med* 43:109–116
- Ishikawa Y, Iwata R, Furumoto S, Takai Y (2005) Automated preparation of hypoxic cell marker [¹⁸F]FRP-170 by on-column hydrolysis. *Appl Radiat Isot* 62:705–710
- Shibahara I, Kumabe T, Kanamori M et al (2010) Imaging of hypoxic lesions in patients with gliomas by using positron emission tomography with 1-(2-[¹⁸F] fluoro-1-[hydroxymethyl]ethoxy)methyl-2-nitroimidazole, a new 18F-labeled 2-nitroimidazole analog. *J Neurosurg* 113:358–368
- Matsumoto K, Szajek L, Krishna MC et al (2007) The influence of tumor oxygenation on hypoxia imaging in murine squamous cell carcinoma using [⁶⁴Cu]Cu-ATSM or [¹⁸F]Fluoromisonidazole positron emission tomography. *Int J Oncol* 30:873–881
- Sorensen M, Horsman MR, Cumming P et al (2005) Effect of intratumoral heterogeneity in oxygenation status on FMISO PET, autoradiography, and electrode Po2 measurements in murine tumors. *Int J Radiat Oncol Biol Phys* 62:854–861
- Mahy P, De Bast M, Gallez B et al (2003) In vivo colocalization of 2-nitroimidazole EF5 fluorescence intensity and electron paramagnetic resonance oximetry in mouse tumors. *Radiother Oncol* 67:53–61
- Tran LB, Bol A, Labar D et al (2012) Hypoxia imaging with the nitroimidazole ¹⁸F-FAZA PET tracer: a comparison with OxyLite, EPR oximetry and 19F-MRI relaxometry. *Radiother Oncol* 105:29–35
- Wang GL, Semenza GL (1995) Purification and characterization of hypoxia-inducible factor 1. *J Biol Chem* 270:1230–1237
- Collingridge DR, Piepmeier JM, Rockwell S, Knisely JP (1999) Polarographic measurements of oxygen tension in human glioma and surrounding peritumoural brain tissue. *Radiother Oncol* 53:127–131
- Kayama T, Yoshimoto T, Fujimoto S, Sakurai Y (1991) Intratumoral oxygen pressure in malignant brain tumor. *J Neurosurg* 74:55–59
- Kaneta T, Takai Y, Iwata R et al (2007) Initial evaluation of dynamic human imaging using ¹⁸F-FRP170 as a new PET tracer for imaging hypoxia. *Ann Nucl Med* 21:101–107
- Chapman JD (1979) Hypoxic sensitizers—implications for radiation therapy. *N Engl J Med* 301:1429–1432
- Krohn KA, Link JM, Mason RP (2008) Molecular imaging of hypoxia. *J Nucl Med* 49(Suppl 2):129S–148S
- Beppu T, Kamada K, Yoshida Y et al (2002) Change of oxygen pressure in glioblastoma tissue under various conditions. *J Neurooncol* 58:47–52
- Brown JM (1979) Evidence for acutely hypoxic cells in mouse tumours, and a possible mechanism of reoxygenation. *Br J Radiol* 52:650–656
- Pistollato F, Abbadì S, Rampazzo E et al (2010) Intratumoral hypoxic gradient drives stem cells distribution and MGMT expression in glioblastoma. *Stem Cells* 28:851–862
- Fischer I, Gagner JP, Law M, Newcomb EW, Zagzag D (2005) Angiogenesis in gliomas: biology and molecular pathophysiology. *Brain Pathol* 15:297–310
- Reischl G, Dorow DS, Cullinane C et al (2007) Imaging of tumor hypoxia with [¹²⁴I]IAZA in comparison with [¹⁸F]FMISO and [¹⁸F]FAZA—first small animal PET results. *J Pharm Pharm Sci* 10:203–211
- Rampling R, Cruickshank G, Lewis AD et al (1994) Direct measurement of pO₂ distribution and bioreductive enzymes in human malignant brain tumors. *Int J Radiat Oncol Biol Phys* 29:427–431
- Piert M, Machulla H, Becker G et al (1999) Introducing fluorine-18 fluoromisonidazole positron emission tomography for the localisation and quantification of pig liver hypoxia. *Eur J Nucl Med* 26:95–109
- Bartlett RM, Beattie BJ, Naryanan M et al (2012) Image-guided PO₂ probe measurements correlated with parametric images derived from ¹⁸F-fluoromisonidazole small-animal PET data in rats. *J Nucl Med* 53:1608–1615